Applied Catalysis B: Environmental 97 (2010) 41–48

Contents lists available at ScienceDirect

Applied Catalysis B: Environmental

journal homepage: www.elsevier.com/locate/apcatb

The effect of Ni on the structure and catalytic behavior of model Pd/$Ce_{0.67}Zr_{0.33}O_2$ three-way catalyst before and after aging

Guangfeng Li[a], Bo Zhao[a,b], Qiuyan Wang[a], Renxian Zhou[a,*]

[a] Institute of Catalysis, Zhejiang University, Hangzhou 310028, PR China
[b] School of Pharmaceutical and Chemical Engineering, Taizhou University, Taizhou 317000, PR China

ARTICLE INFO

Article history:
Received 20 January 2010
Received in revised form 10 March 2010
Accepted 15 March 2010
Available online 20 March 2010

Keywords:
$Ce_{0.67}Zr_{0.33}O_2$
Pd
Ni
Aging
Three-way catalyst

ABSTRACT

$Ce_{0.67}Zr_{0.33}O_2$ (CZ) doped by nickel oxide with different content and the corresponding Pd-only three-way catalysts before and after aging has been prepared and characterized. The investigations show that CZ doped with nickel oxide obviously results in more active fresh catalysts with enhanced textural properties, but suffers from a net loss of activity after aging. The introduction of Ni promotes the reducibility of samples, causing the enhancement of oxygen storage capacity (OSC) of fresh samples. CZNi(3%) exhibits better textural and structural properties because of the formation of more homogeneous Ce–Zr–Ni–O ternary solid solution, which promotes the interaction between Ce–Zr and Ni. However, the thermal aging leads to a loss of surface area and a significant decrease of the reducibility and OSC, except for CZNi(3%). Only Pd/CZNi(3%) represents better catalytic activity after aging. It reveals that the catalytic behavior of these bimetallic systems is strongly affected by the nature of support.

1. Introduction

Three-way catalysts (TWCs) have been widely used to diminish the environmental impact of pollutants emitted by gasoline engine powered vehicles [1–3]. TWCs can work efficiently to reduce NO as well as to oxidize CO and hydrocarbons (HC) in a narrow window of air-to-fuel ratio (A/F), close to the stoichiometric point [3–5]. Classical components of these systems usually include Rh, Pt, and/or Pd as active metals, ceria as promoter, and high surface alumina as the support [6,7]. In recent years, ceria–zirconia mixed oxide systems have been considered as substitutes of ceria on the basis of their greater oxygen storage capacity (OSC) after thermal sintering [7–10], which could potentially decrease the cold-start emissions mainly by allowing the catalyst to be located in positions closer to the engine manifold with minimum system deactivation being produced [2,11]. Concerning the active metal components, the use of Pd as the only active metal in TWCs has received considerable attention on the basis of economic factors (i.e., the high cost and scarcity of Rh), the availability of cleaner fuels and its remarkable activity for hydrocarbon and CO oxidation reactions [2,12]. However, Pd-based catalysts display limitations with respect to their performance for NO reduction reactions [13,14]. Modification of Pd by addition of a second, cheaper metal would appear to offer a viable solution from both an economical and catalytic point of view [15,16]. In recent years, the introduction of transition metals into TWCs [17–19], which promoted the NO reduction and achieved the lower light-off temperature during the cold-start phase, has earned much attention in Pd-only TWCs area [20–23]. Thus, recent literature mainly reports the effect of transition metals on the catalytic activity over Pd-transition metal co-impregnated TWCs. Promising results have been obtained by using Mn, Cr or Cu, which have been attributed to the formation of the corresponding alloys. Moreover, in the case of Mn, effects involving alloy formation and Pd–MnO_x interactions have been observed [24–26]. Ana Iglesias-Juez et al. [16] investigated the promoting effect of base metals (Cr, Cu, Ni) on CO and NO elimination over Pd-based (Ce, Zr)O_x-supported catalysts. Among the base metals tested, Ni appeared to exert the least influence on the noble metal state/behavior after calcinations. While Cr and Cu appeared to interacting with Pd in the calcined state, leading to a reduction in the temperature at which Pd was converted to Pd(0) with simultaneous formation of a binary PdM alloy during the reaction run. Reports by researchers have shown the beneficial effect of establishing interactions between Pd and Ni, especially on enhancing NO_x conversion under stoichiometric or rich atmospheres [20,27,28]. But the sintering phenomenon of catalysts could be strongly happened after aging, which made the deactivation of these Pd-transition metals co-impregnated TWCs.

Recently, much attention has been paid to incorporation of transition metals into the CeO_2–ZrO_2 lattice, which can improve both the textural stability and the reducibility of metal-loaded CeO_2–ZrO_2, such as CeO_2–ZrO_2 doped with Mn [19], Cu [18,23], Fe [29,30] and so on. Homogeneity of the solid solution, structural

* Corresponding author. Tel.: +86 571 88273290; fax: +86 571 88273283.
E-mail address: zhourenxian@zju.edu.cn (R. Zhou).

0926-3373/$ – see front matter.
doi:10.1016/j.apcatb.2010.03.022

features and composition are key factors in successful redox catalyst design. Moreover, this ternary solid solution could improve the thermal stability and enhance the migration and exchange of oxygen species by storing and releasing oxygen. In this work, a series of CZ doped by nickel oxide with different content (0.5%, 1%, 3%, 5%) were prepared by co-precipitation method. In order to study the effect of Ni on the structure and catalytic behavior of model Pd/CZ three-way catalyst before and after aging, a multi-technique approach involving X-ray diffraction (XRD), N_2 adsorption, X-ray photoelectron spectrometer (XPS), oxygen storage capacity (OSC), H_2-temperature-programmed reduction (H_2-TPR) and catalytic test were used to characterize the samples and to evaluate the catalytic performance.

2. Experimental

2.1. Catalyst preparation

$Ce_{0.67}Zr_{0.33}O_2$ doped by nickel oxide with different content was prepared through a co-precipitation route. The doping of nickel oxide was fixed at x wt% (x = 0, 0.5, 1, 3, 5). $ZrO(NO_3)_2$, $Ce(NO_3)_3$ and $Ni(NO_3)_2{\cdot}6H_2O$ were used as metal precursors. The required amounts of $ZrO(NO_3)_2$, $Ce(NO_3)_3$ and/or $Ni(NO_3)_2{\cdot}6H_2O$ were dissolved in water. The NaOH solution was added dropwise to the solution of metal precursors to maintain the pH at about 9.5. The obtained slurry was aged at room temperature for 12 h, and then filtered, washed with deionized water and dried under supercritical condition in ethanol (265 °C, 7.0 MPa) for 2 h. The samples were calcined at 500 °C in air for 4 h to obtain fresh support. All of the obtained supports were pressed into pellets, crushed and sieved to 40–60 meshes. The supports were designated as CZ, CZNi(0.5%), CZNi(1%), CZNi(3%), CZNi(5%), respectively. All the samples were calcined at 1000 °C for 4 h in air to obtain aged supports.

Five Pd-only catalysts with different mixed oxides as supports (Pd/CZNi(x wt%), x = 0, 0.5, 1, 3, 5) were prepared by incipient wetness impregnation method with aqueous solutions of H_2PdCl_4 as metal precursors. Pd content was 0.5 wt%. The impregnated sample was reduced with hydrazine hydrate solution for 2 h, washed several times with deionized water until no Cl^- ions detected in the filtered solution, and then dried at 110 °C for 4 h followed by calcination at 500 °C for 2 h to obtain fresh catalyst. The catalysts were further calcined at 1000 °C for 4 h in air to obtain aged catalyst.

2.2. Catalytic activity measurement

Catalytic tests were carried out with a fixed-bed continuous flow reactor. The catalyst (0.2 ml) was held in a quartz tube by packing quartz wool at both ends of the catalyst bed. The reaction mixture containing NO(0.1%), NO_2(0.03%), C_3H_6(0.067%), C_3H_8(0.033%), CO(0.75%), O_2(0.745%) and balance Ar was fed to the reactor at a GHSV of 43,000 h^{-1}. The effluent gas was analyzed by on-line Fourier transform infrared spectrophotometer (BRUKER EQ55) equipped with a multiple reflection transmission cell (Infrared Analysis Inc.; path length 10.0 m). All spectra were taken at a resolution of 2 cm^{-1} for 128 scans. The air/fuel ratio experiments were carried out at 400 °C. The concentration of O_2 was adjusted in the tests of air/fuel ratio from 850 to 8440 ppm. The λ value of the simulated exhaust, which represents the ratio between the available oxygen and the oxygen needed for full conversion to CO_2, H_2O and N_2, is defined as $\lambda = \{2[O_2] + [NO] + 2[NO_2]\}/\{9[HC] + [CO]\}$, $\lambda = 1$ was at stoichiometry and the corresponding concentration of O_2 was 7450 ppm.

2.3. Characterization techniques

X-ray diffraction (XRD) measurement was performed on an ARL X'TRA X-ray Diffractometer (Thermo Eelctron Corporation, USA), with Cu Kα radiation, operating at 40 kV and 40 mA. Spectra were collected using a step size of 0.04° and a counting time of 5 s per angular abscissa in the range of 20–80° (2θ).

The textural properties were determined by N_2 adsorption using TriStar Π 3020 (Micromeritics Inc.). The sample (0.15 g) was degassed at 200 °C for 3 h under vacuum, and N_2 adsorption was carried out at −196 °C.

X-ray photoelectron spectroscopy (XPS) analysis was performed on a PHI5000c spectrometer with the Mg Kα radiation (1253.6 eV), operating at 14 kV and 20 mA. The surface charging effect was corrected by fixing the C 1s peak at a binding energy of 284.6 eV.

Hydrogen-temperature-programmed reduction (H_2-TPR) measurements were carried out using a thermal conductivity detector (TCD). Each sample (50 mg) was pretreated at 300 °C for 30 min in air and cooled down to room temperature or −40 °C in N_2. The gas flow was then switched to 5% H_2/Ar, and the sample was heated to 900 °C at a rate of 10 °C min^{-1}.

Oxygen storage capacity measurement was carried out using CHEMBET-3000 (Quantachrome Co.). The sample (100 mg) was reduced at 550 °C for 60 min in H_2 (10 ml/min), then cooled down to the reaction temperature and purged with He (30 ml/min) for 20 min. A given amount of O_2 (0.15 ml) was pulsed every 5 min until the intensity of the peak reached a constant value.

3. Results and discussion

3.1. XRD and BET

A detailed investigation of the textual and structural characterization between CZ and CZNi(x wt%) before and after aging are conducted in Figs. 1 and 2 and Table 1, respectively. The XRD patterns of the fresh and aged supports are depicted in Fig. 1. For fresh samples of CZNi (Fig. 1A), the mainly cubic fluorite-structured phase of CeO_2 are detected while NiO or other nickel oxide phases are not visible. Moreover, XRD peaks become broader with nickel

Table 1
Textural and structural properties of fresh and aged $Ce_{0.67}Zr_{0.33}O_2$ mixed oxides doped by nickel oxide with different content.

Samples		Average pore diameter (nm)	Pore volume (m^3/g)	S_{BET} (m^2/g)	Phase*	Crystallite size (nm)
Fresh	CZ	20.87	0.7281	122.0	c	7.9
	CZNi(0.5%)	20.35	0.8025	122.7	c	7.9
	CZNi(1%)	16.74	0.7698	147.5	c	7.0
	CZNi(3%)	23.25	0.9701	152.1	c	6.2
	CZNi(5%)	19.39	0.9227	154.8	c	7.3
Aged	CZ	32.86	0.1075	26.1	c + t	31.6
	CZNi(0.5%)	29.73	0.0612	17.8	c + t	36.8
	CZNi(1%)	24.64	0.0792	18.1	c + t	35.4
	CZNi(3%)	46.34	0.1252	30.1	c + t	23.8
	CZNi(5%)	37.65	0.1169	28.5	c + t	27.9

* c: cubic phase; t: tetragonal phase.

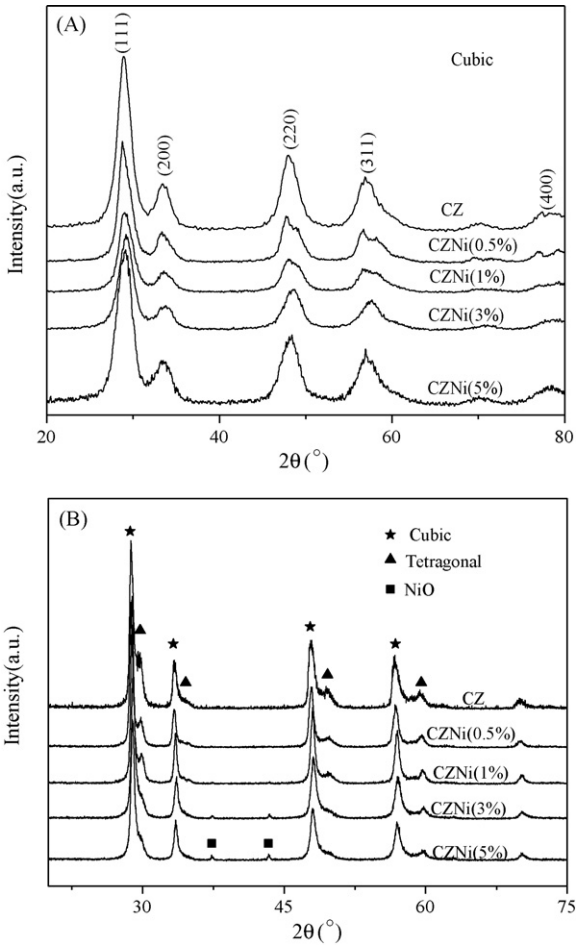

Fig. 1. XRD characterization of fresh (A) and aged (B) $Ce_{0.67}Zr_{0.33}O_2$ mixed oxides doped by nickel oxide with different content.

oxide content increasing from 0.5% to 5%, corresponding to the decrease of the crystal size calculated from the (1 1 1) plane (2θ = ca. 28.7°) using Scherrer's equation in Table 1. The cell parameter of fresh CZNi(0.5%), CZNi(1%), CZNi(3%), and CZNi(5%) is 0.5394, 0.5359, 0.5306 and 0.5382 nm, respectively, which is smaller than CZ (0.5407 nm). It may be due to the fact that the ion radius of Ni^{2+} (0.069 nm) is smaller than that of Ce^{4+} (0.097 nm)/Ce^{3+} (0.112 nm) and Zr^{4+} (0.084 nm). Incorporation of Ni^{2+} into the CZ lattice by replacing of Ce^{4+}/Ce^{3+} or Zr^{4+} leads to the shrinkage of the lattice

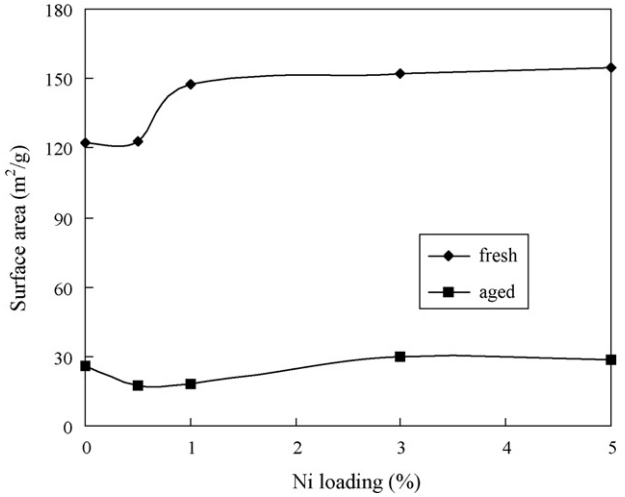

Fig. 2. Surface area of samples as a function of nickel oxide loading.

parameter. It indicates the formation of Ce–Zr–Ni–O ternary solid solution between Ce, Zr and Ni. Additionally, the best symmetrical peaks and smallest crystal size are observed when the content of doped nickel oxide is 3%, confirming the formation of more homogeneous Ce–Zr–Ni–O ternary solid solution. Furthermore, the average pore diameter is obviously increased by the CZNi(3%) solid solution. After aging at 1000 °C, as shown in Fig. 1B, the diffraction peaks become more intense and more symmetrical, clear and well defined for all Ni containing samples, indicating the growth of the nanocrystals [31] with the increasing of the crystallite size. And phase segregation occurs for the aged samples, especially for CZ, CZNi(0.5%) and CZNi(1%), together with the cubic and tetragonal CZ crystal phase [32,33]. Moreover, the XRD profile of CZNi(5%) sample clearly shows peaks assigned to the NiO phase. For aged CZNi(3%) support, no evident phase segregation occurs and only weak peaks due to nickel oxide appear.

Fig. 2 presents the surface area of fresh and aged samples with different nickel oxide loading. For fresh supports, the introduction of Ni strongly enhances the surface area of the CZ, expect for CZNi(0.5%). However, no clear enhancement of the surface area occurs when the content of doped nickel oxide increased from 3% to 5%. Combined with the results of Fig. 1 and Table 1, we point out that the optimum amount of nickel oxide loading is 3%. Aging is accompanied by a large drop in surface area and a corresponding increase in crystallite size (Table 1) for all samples. The presence of Ni with low content (0.5%, 1%) within CZ lattice does not modify the textural stability of CZ. However, when the content of doped nickel oxide is 3%, the surface area of aged CZ is obviously improved. Moreover, the average pore diameters increase after aging. Furthermore, when the content of doped nickel oxide increases from 3% to 5%, the surface area of aged CZNi(5%) support decreases contrarily. It is reasonable to propose that the structural and textural stabilities of ternary solid solution [30] are improved by introduction of nickel oxide with the content of 3%. Combined with the above discussions, we conclude that the improvement of textural and structural stability of aged CZNi(3%) is possibly correlated to the formation of more homogeneous Ce–Zr–Ni–O ternary solid solution in fresh CZNi(3%) support.

3.2. XPS

The composition of the outermost surface layers is investigated by means of the XPS technique. The surface composition and atomic ratios obtained by XPS are listed in Table 2. For fresh CZNi samples, the surface atom ratios of Ce/Zr are surely higher than that of fresh CZ, in respect that the Ni species disperse on the surface of the oxide particles. This also means that part of Zr atoms of the surface layer is replaced by Ni atoms. As more Ni atoms are distributed on the surface instead of being incorporated into the bulk, an obvious shrinkage of the lattice parameter is detected as mentioned above, especially for CZNi(3%). The same Pd surface composition is obtained over these catalysts. This, however, cannot exclude the detection limit of this technique owing to the low loading of Pd metal (0.5%) and the disturbance of Zr 3p. In respect that the Zr $3p_{1/2}$ component of the Zr 3p doublet is located at ca. 346.0 eV, overlapping the Pd 3d peak. The Zr $3p_{1/2}$ core level predominates in this XPS region for the samples with low Pd concentration [34,35]. It is of interesting to find that the surface content of Ce experiences remarkably decrease after aging and only Pd/CZNi(3%) shows a higher surface Ce content than that of Pd/CZ. It may be due to the strongly sintering of the catalyst after aging at 1000 °C. In addition, the migration of Zr from the bulk to the surface during aging process can be indicated according to the decrease of Ce/Zr ratios [36].

The spectra of the Ni 2p core level over fresh and aged catalysts are shown in Fig. 3. For all samples examined, a main peak at ca. 858 eV is observed in the Ni $2p_{3/2}$ binding energy region. Further-

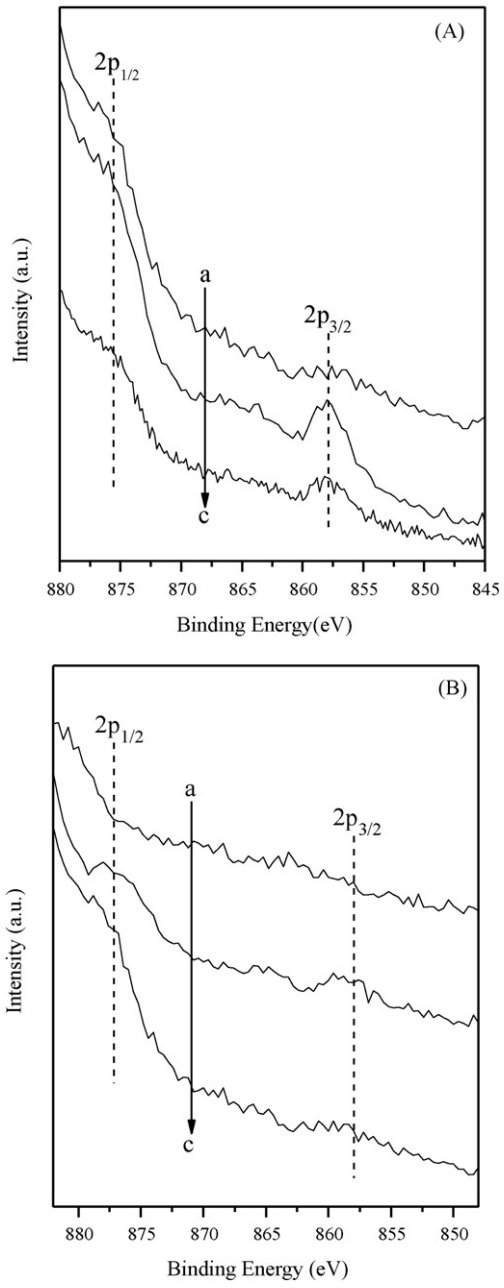

Fig. 3. Ni 2p spectra for the fresh (A) and aged (B) Pd/CZNi(*x* wt%) catalysts: (a) Pd/CZNi(1%), (b) Pd/CZNi(3%), (c) Pd/CZNi(5%).

more, the peak shifts to higher energy compared to the binding energy of Ni and NiO. It may be due to the fact that Ni 2p levels are sensitive to the interaction between Ce–Zr and Ni. No change is observed in the position of the Ni $2p_{3/2}$ peak even though the amount of Ni loading is high. However, the intensity of the peak is different, the sequence is Pd/CZNi(3%) > Pd/CZNi(5%) > Pd/CZNi(1%). It may be correlated to the formation of more homogeneous Ce–Zr–Ni–O ternary solid solution in fresh CZNi(3%) support which promotes the interaction between Ce–Zr and Ni. The intensity of the signal over aged samples is weakened in contrast to that of fresh samples, but little difference in Ni 2p species is observed among aged samples. The sintering may be the major factor that leads to the decrease of the intensity, which can be observed from the crystal sizes in Table 1 [19]. What's more, the sequence of the peak intensity follows the same order for aged samples as that for fresh catalysts, that is Pd/CZNi(3%) > Pd/CZNi(5%) > Pd/CZNi(1%). It demonstrates that the more homogeneous Ce–Zr–Ni–O ternary solid solution promotes the interaction between Ce–Zr and Ni and exhibits better thermal resistance, which can be confirmed by the surface area of aged supports (Fig. 2).

3.3. H_2-TPR

The reducibility of fresh and aged samples is investigated and a series of consecutive TPR profiles are illustrated in Figs. 4 and 5. Fig. 4A gives H_2-TPR profiles of fresh CZ doped by nickel oxide with different content. For CZ, two strong reduction peaks appear in its TPR profile with two maximum at 340 and 553 °C (referred to α, β), which are ascribed to the reduction of surface and subsurface oxygen [10,37,38]. Obviously, these peaks are shifted to lower temperature by the presence of nickel oxide. It is due to the effect of strong metal–support interaction between CZ and nickel metal which enhances the reduction of the support. Furthermore, these two peaks shift to the lowest temperature and the intensity of the peaks become strongest for the CZNi(3%) sample. Consequently, it is assumed that the formation of more homogeneous Ce–Zr–Ni–O ternary solid solution in fresh CZNi(3%) support enhances the metal-support interaction between CZ and Ni, confirming the XPS results. After aging at 1000 °C, as shown in Fig. 4B, the intensity of the peaks ascribed to the reduction of surface and subsurface oxygen become weak compared with those of fresh supports, due to the sintering of supports at high temperature. The introduction of Ni also enhances the reduction of the aged support, especially for aged CZNi(3%) and CZNi(5%). Moreover, other small reduction peaks (287 and 569 °C) are observed over aged CZNi(5%) support, which possibly ascribe to the reduction of small crystallites and NiO species according to the XRD results (Fig. 1B).

Fig. 5 presents H_2-TPR profiles of fresh and aged catalysts. Previous investigations have reported that palladium oxide is reduced to palladium metal on exposure to H_2 at room temperature [39]. From Fig. 5A, it can be seen that all of the fresh catalysts exhibit one or two dominant lower temperature reduction feature with

Table 2
Surface composition and surface atom ratios in the fresh and aged Pd/CZNi(*x* wt%) catalysts derived from XPS analyses.

Sample		Surface composition (at%)					Ce/Zr	Ni/Ce + Zr	Pd/Ce ($\times 10^{-4}$)
		Ce 3d	Zr 3d	Ni 2p	Pd 3d	O 1s			
Fresh	Pd/CZ	13.7	7.38	–	0.01	78.91	1.86	–	7.0
	Pd/CZNi(1%)	16.2	7.29	0.3	0.01	76.2	2.22	0.011	5.0
	Pd/CZNi(3%)	15.3	6.5	0.5	0.01	77.69	2.35	0.023	6.0
	Pd/CZNi(5%)	13.3	6.2	0.6	0.01	79.8	2.14	0.031	7.0
Aged	Pd/CZ	8.58	8.34	–	0.01	83.07	1.03	–	12
	Pd/CZNi(1%)	6.31	7.31	0.3	0.01	86.07	0.86	0.022	16
	Pd/CZNi(3%)	6.71	5.82	0.4	0.02	87.07	1.15	0.032	30
	Pd/CZNi(5%)	6.7	7.2	0.6	0.01	85.49	0.93	0.043	15

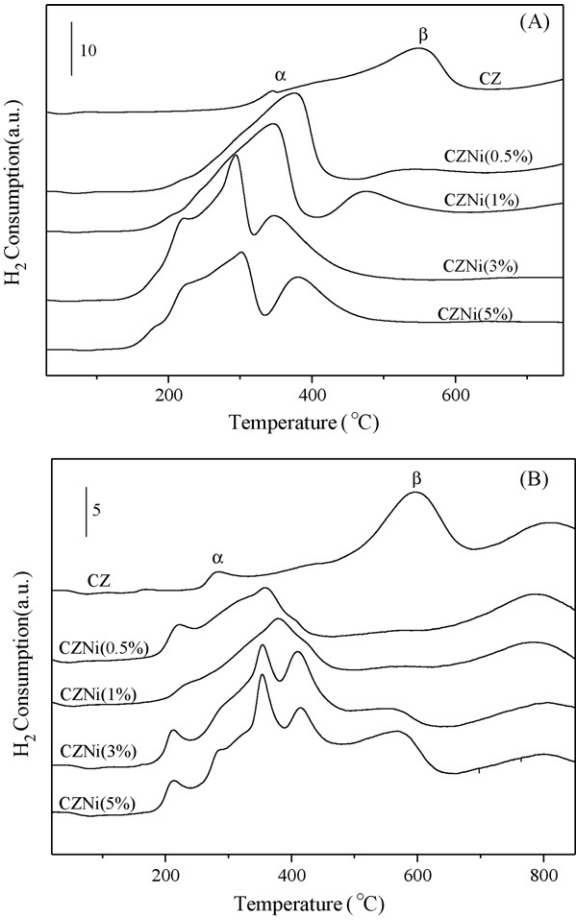

Fig. 4. H_2 consumption profiles during H_2-TPR over fresh (A) and aged (B) $Ce_{0.67}Zr_{0.33}O_2$ mixed oxides doped by nickel oxide with different content.

maxima at 80 and 102 °C (peak a and b), which can be attributed to the reduction of PdO species highly dispersed on the surface of the support and formed on the interaction between PdO and the support [40], respectively. What have been known to us is that the introduction of Ni strongly enhances the surface area of CZ, and the phenomenon that the introduction of Ni promotes the reduction of PdO species highly dispersed on the surface of support is also observed, especially for the Pd/CZNi(0.5%), Pd/CZNi(1%) and Pd/CZNi(5%). However, for Pd/CZNi(3%) catalyst, the presence of Ni promotes the reduction of PdO species formed on the interaction between PdO and the support. This behavior is attributable to the strong interaction between PdO and CZNi(3%) support. Combined with the results of Section 3.1, we estimate that the promotional effect on the reduction of PdO species is possibly correlated to the formation of more homogeneous Ce–Zr–Ni–O ternary solid solution in fresh CZNi(3%) support.

After aging, the TPR profiles of catalysts (Fig. 5B) also exhibit the reduction peaks (a and b) of PdO species. The negative peak at ca. 80 °C is generally attributed to the decomposition of palladium hydride when reduced Pd is exposed to H_2 furthermore [41]. The intensity of the reduction peaks of PdO species decrease obviously over aged Pd/CZNi(0.5%) and Pd/CZNi(1%) catalysts, which are attributed to the low dispersion of PdO species caused by the serious sintering during aging process. On the contrary, the intensity of the reduction peaks of PdO species, especially for the peak a, increase obviously over aged Pd/CZNi(3%) and Pd/CZNi(5%) catalysts. It is possibly due to the higher surface area of these two catalysts after aging. What is more, three peaks denoted as c, d and e appear over aged catalysts, which are also associated with the reduction of surface small crystallites and partial reduction of subsurface larger crystallites [32,39]. And the intensity of these three peaks increase with the increasing of doped Ni loading. Generally, it is known that the TPR behavior of these mixed oxides depend on different factors such as pre-treatment conditions, degree of sintering and phase structure. Therefore, we speculate that the appearance of these peaks correlates to the presence of NiO species and the degree of sintering.

3.4. Oxygen storage capacity (OSC)

The oxygen storage capacity (OSC) of sample is regarded as one of the most important parameters to evaluate the applicability of materials to rapidly switching between lean and rich conditions. The OSC of ceria–zirconia is intrinsic to its structure [42,43,44]. Moreover, intrinsic microstructure variation of ceria–zirconia on the Zr coordination could be correlated to the oxygen mobility [45]. This is the primary reason why ceria–zirconia materials are used in TWCs in place of pure ceria [38]. Furthermore, the light-off catalytic performance is improved by the enhancement of oxygen mobility of the sample at lower temperature. Fig. 6 displays the OSC of samples as a function of Ni loading at 200 °C. From Fig. 6, it can be seen that the introduction of Ni clearly enhances the OSC of fresh supports and catalysts, respectively. Moreover, the OSC of the CZNi(3%) is higher than that of others. Combination with the H_2-TPR results, we conclude that the OSC properties of CZNi samples are related to the reducibility of samples. It is known that the sensitivity of the

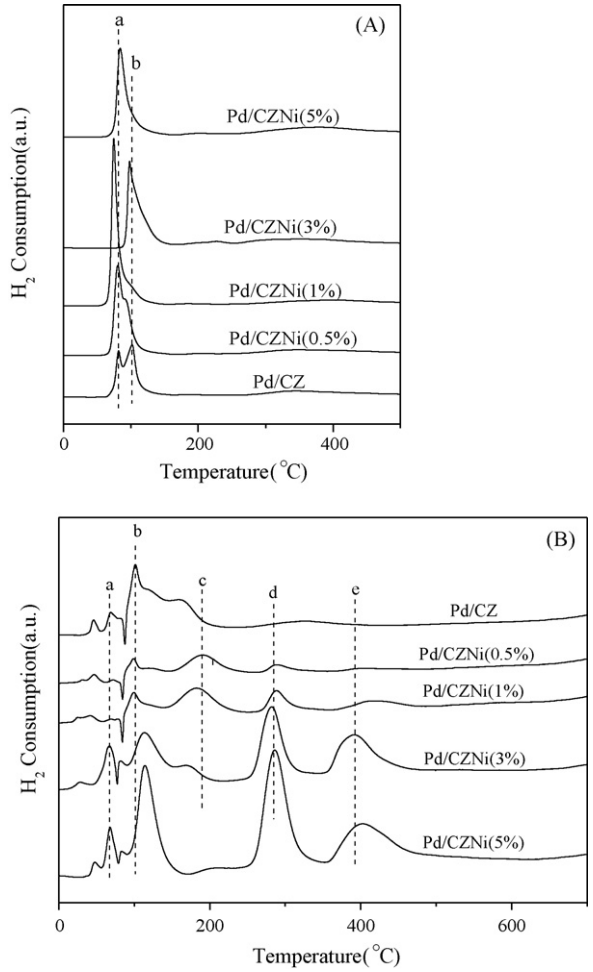

Fig. 5. H_2 consumption profiles during H_2-TPR over fresh (A) and aged (B) Pd/CZNi(x wt%) catalysts (x = 0, 0.5, 1, 3, 5).

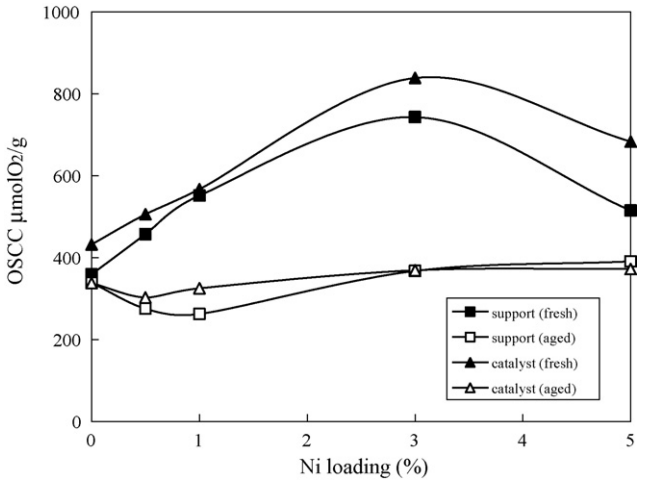

Fig. 6. Oxygen storage capacity of samples as a function of nickel oxide loading at 200 °C.

OSC characteristics to their surface area and bulk structure is an important aspect of the OSC behavior of the ceria–zirconia-based materials [46]. Therefore, the improvement of OSC of CZNi(3%) may be ascribed to the higher surface area and the more homogeneous structure of Ce–Zr–Ni–O ternary solid solution of this support. The oxygen vacancies relating to structure modification is increased by the formation of more homogeneous structure, which has been proposed to explain the OSC promotion. On the other hand, defects play another role in the oxygen storage process when noble metal is supported on ceria–zirconia, which is the usual application in practice [38]. Oxidation of noble metal in Pd/ceria–zirconia catalyst reflects electron transfer from metal to ceria–zirconia, indicating slightly reduced Ce associated with oxygen vacancy formation [38,47]. It explains the improvement of oxygen storage capacity of catalysts compared to that of corresponding supports.

After aging at 1000 °C, as shown in Fig. 6, the OSC of the samples decrease obviously, possibly due to the sintering of the support that makes the decrease of oxygen vacancies. Nevertheless, the OSC of aged CZNi(3%) and CZNi(5%) are higher than that of aged CZ. Contrarily, the OSC of aged CZNi(0.5%) and CZNi(1%) are lower than that of aged CZ. It is worth pointing out that the change of the OSC is correlated to the change of surface area of aged supports. For aged CZNi(5%) sample, the increase of OSC is possibly ascribed to the higher surface area compared to aged CZNi(0.5%) and CZNi(1%) supports. For aged CZNi(3%), the increase of OSC may be attributed to the higher surface area, which is due to the more homogeneous structure of fresh support. Combined with the OSC of the fresh and aged samples, we prove that the OSC behavior of the ceria–zirconia-based materials is sensitive to their structure and surface area.

3.5. Catalytic activity of the catalysts

Fig. 7 presents the conversions of HC, CO, NO and NO_2 under stoichiometric $CO + HC + NO_x + O_2$ reaction conditions over fresh Pd/CZNi(*x* wt%) catalysts. All the catalysts examined are active in promoting catalytic activity in the range of temperature from ca. 100 to 400 °C, especially for CO, NO and NO_2 conversion. Table 3 summarizes the light-off ($T_{50\%}$) and full-conversion temperature ($T_{90\%}$) of CO, HC, NO and NO_2 as well as the width of the window

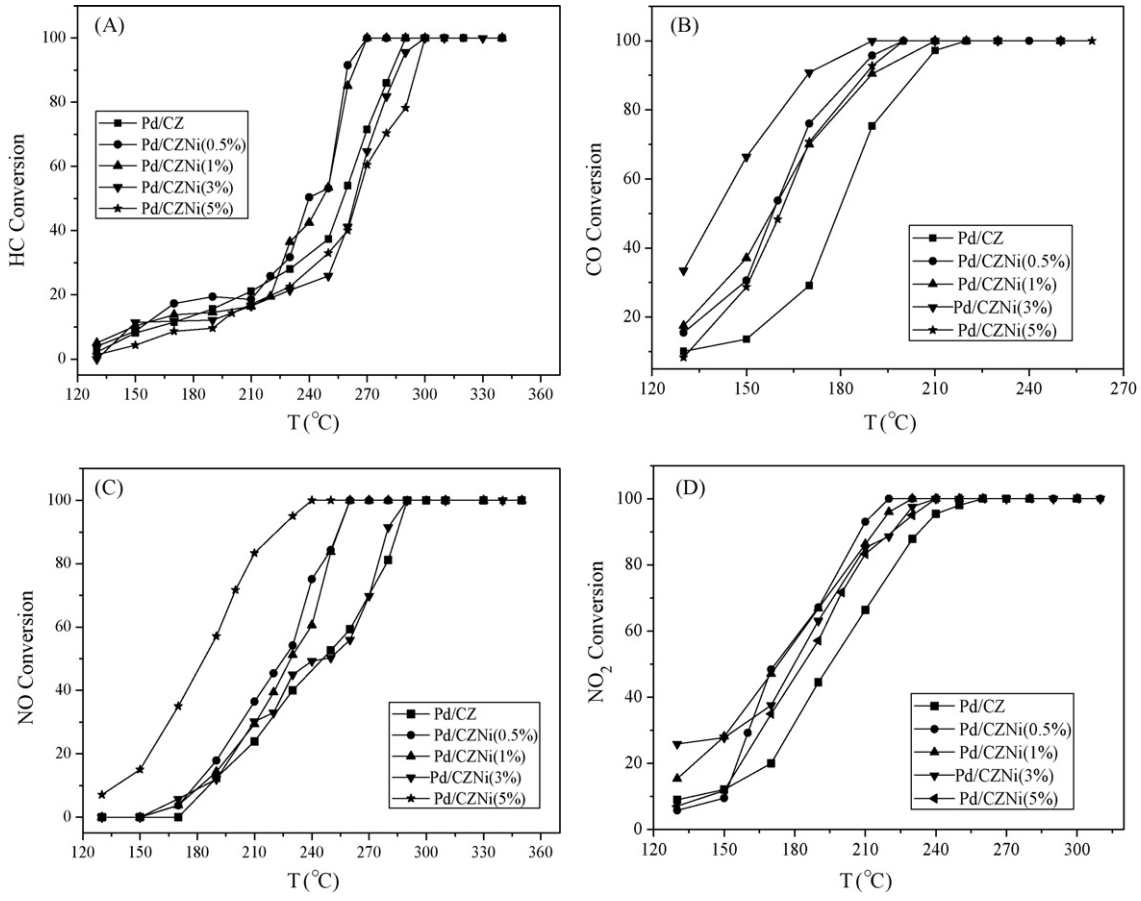

Fig. 7. Conversion of HC (A), CO (B), NO(C) and NO_2 (D) as a function of reaction temperature under stoichiometric $CO + NO_x + HC + O_2$. *Reaction condition*: NO(0.1%)–NO_2(0.03%)–C_3H_6(0.067%)–C_3H_8(0.033%)–CO(0.75%)–O_2(0.745%) in Ar over fresh catalysts.

Table 3
Light-off temperature and full-conversion temperature of CO, HC, NO and NO_2 and the width of the window (W) over fresh Pd/CZNi(x wt%) catalysts.

Catalyst	$T_{50\%}$ (°C)				$T_{90\%}$ °C)				W
	HC	CO	NO	NO_2	HC	CO	NO	NO_2	
Pd/CZ	258	178	246	195	283	204	284	233	0.221
Pd/CZNi(0.5%)	240	158	225	171	260	184	254	207	0.243
ΔT^*	18	20	21	24	23	20	30	26	
Pd/CZNi(1%)	246	157	229	173	263	189	254	213	0.238
ΔT	12	21	17	22	20	15	30	20	
Pd/CZNi(3%)	263	140	240	180	285	170	279	221	0.250
ΔT	−5	38	6	15	−2	34	5	12	
Pd/CZNi(5%)	264	161	184	184	295	187	221	221	0.232
ΔT	−6	17	62	11	−12	17	63	12	

* $\Delta T = T(\text{Pd/CZ}) - T(\text{Pd/CZNi}(x\text{ wt\%}))$.

(W) over Pd/CZNi catalysts. In our experiments, we also test the conversions of CO, HC and NO_x under different air/fuel ratios (λ = 0.2, 0.4, 0.6, 0.8, 1.0, 1.04, 1.07, 1.1, 1.15). The left side of the theoretical stoichiometric value (λ = 1) is lean oxygen, and the right is rich oxygen. W (λ value width) acts as another scale to evaluate catalyst property when CO, HC and NO_x conversions all reach to 80% under rich and lean conditions. For example, the upper limit of the stoichiometric windows is limited by NO_x conversion under rich condition; the lower limit is limited by CO conversion under lean conditions for all samples. The upper limit subtracts the lower limit of λ is W value. Furthermore, the wider the W value is, the broader the three-way working window is. From Table 3, it can be seen that the introduction of Ni clearly promotes the catalytic activity and decreases the light-off temperature of the catalysts. Furthermore, Pd/CZNi(3%) catalyst exhibits the best catalytic activity for CO elimination and the widest operation window. This behavior could be correlated with the structural features rather than the surface area. It may be due to the fact that the formation of more homogeneous Ce–Zr–Ni–O ternary solid solution in fresh CZNi(3%) promotes the reducibility and the OSC of the sample, which further enhances the catalytic behavior of the catalyst. For Pd/CZNi(5%) catalyst, it exhibits the best catalytic activity for NO elimination, suggesting that the doping of high amount of Ni favors the reduction of the NO. Moreover, Pd/CZNi(0.5%) and Pd/CZNi(1%) exhibit the similar

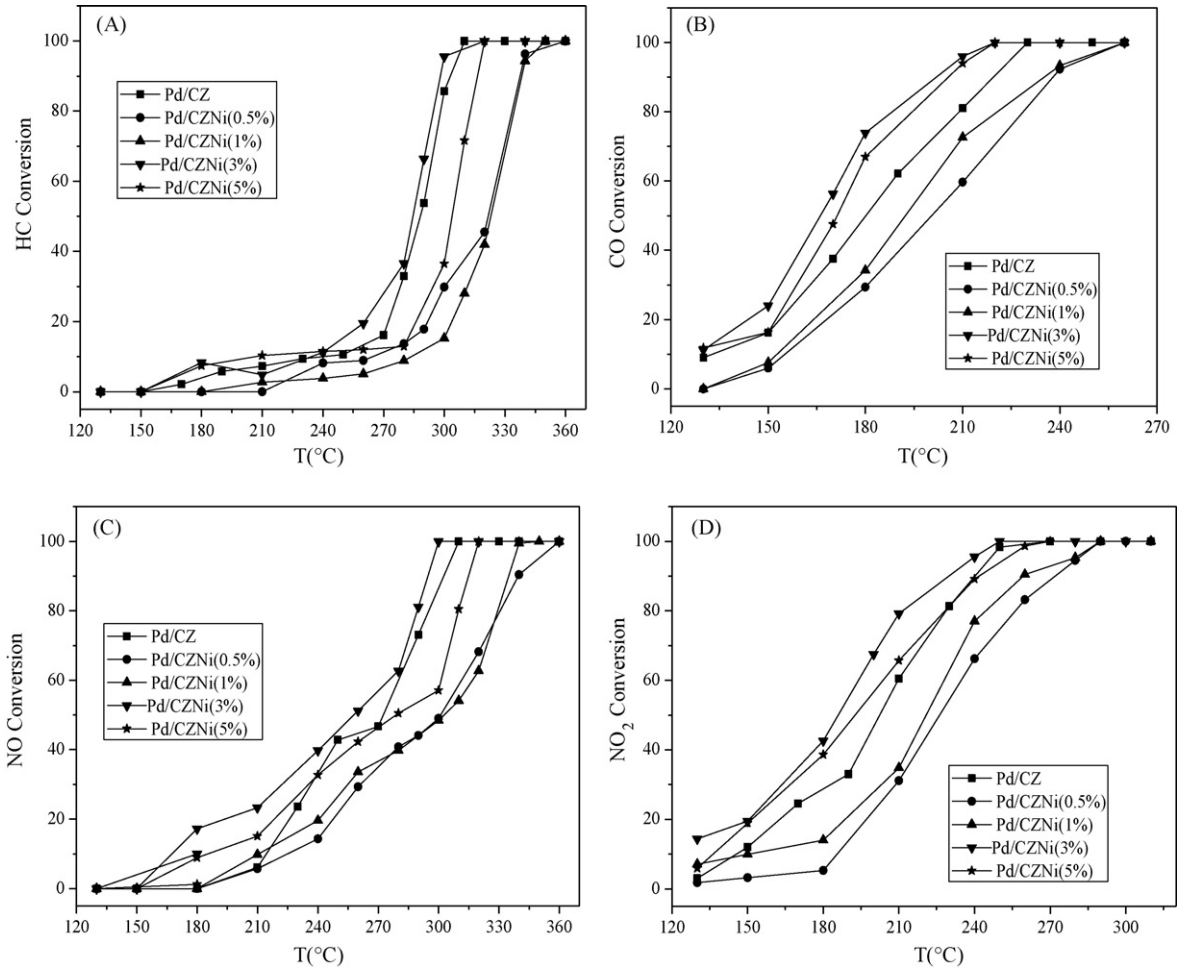

Fig. 8. Conversion of HC (A), CO (B), NO (C) and NO_2 (D) as a function of reaction temperature under stoichiometric $CO + NO_x + HC + O_2$. *Reaction condition*: NO(0.1%)–NO_2(0.03%)–C_3H_6(0.067%)–C_3H_8(0.033%)–CO(0.75%)–O_2(0.745%) in Ar over aged catalysts.

catalytic activity for the elimination of four species. Better catalytic activity can be seen over fresh catalysts, but a large drop of activity is observed over catalysts after calcination at 1000 °C, especially for aged Pd/CZNi(0.5%) and Pd/CZNi(1%) catalysts. Fig. 8 gives the conversions of CO, HC, NO and NO_2 as a function of temperature under stoichiometric CO + HC + NO_x + O_2 reaction conditions over aged Pd/CZNi catalysts. Compared with aged Pd/CZ catalyst, only aged Pd/CZNi(3%) catalyst exhibits a relatively better catalytic activity, corresponding to the decrease of the light-off temperature and the promotion of the full conversion. Moreover, the window of activity of the catalyst (not given) becomes wider. The second good one is the aged Pd/CZNi(5%) catalyst. Aged Pd/CZNi(0.5%) and Pd/CZNi(1%) exhibit the worst catalytic activity. From the above discussions, we have concluded that the thermal aging leads to the loss of surface area as detected by N_2 adsorption and simultaneously a significant decrease of the reducibility and the OSC. Only aged Pd/CZNi(3%) and Pd/CZNi(5%) exhibit the bigger surface area and the OSC as well as better reducibility. It is worth noting that the deactivation seems to be related to two different phenomena: (1) sintering of the metal particles results in a decrease of surface area and the reducibility; (2) the decrease of CZ surface area leads to the loss of the OSC. Combined with the catalytic performance of fresh catalysts, we propose that the catalytic behavior of these bimetallic systems is strongly affected by the nature of support. The enhancement of the catalytic performance of Pd/CZNi may be due to the fact that the formation of more homogeneous Ce–Zr–Ni–O ternary solid solution in fresh CZNi promotes the reducibility and the OSC of the sample, which further enhances the catalytic behavior of the catalyst. Moreover, the decrease of the reducibility and the OSC of samples results in the deactivation of the aged catalysts. It indicates that the catalytic activity of catalyst could be correlated with the properties of the samples.

4. Conclusion

To sum up the above discussions, the following conclusions can be drawn: CZ doped with nickel oxide obviously results in more active fresh Pd-only three-way catalysts with enhanced textural properties. The introduction of Ni strongly improves the surface area and decreases the crystallite size of the CZ. It is worthwhile to note that the introduction of Ni promotes the reducibility of the supports and catalysts, causing the enhancement of the oxygen storage capacity of fresh samples at lower temperature. It is of interesting to confirm that CZNi(3%) exhibits better textural and structural properties because of the formation of more homogeneous Ce–Zr–Ni–O ternary solid solution, which promotes the interaction between Ce–Zr and Ni, confirmed by the XPS results. Aging is accompanied by an evident loss of surface area together with a significant decrease of the reducibility and the OSC. Moreover, the thermal aging leads to a net loss of activity of catalysts. Compared to aged CZ, only aged CZNi(3%) support represents better textural and structural properties as well as OSC promotion. Furthermore, Pd/CZNi(3%) catalyst exhibits better catalytic activity after aging. Based on the above experimental facts, we speculate that the decrease of the reducibility and the OSC of samples results in the deactivation of the aged catalysts. From the above discussions, it also reveals that the catalytic behavior of these bimetallic systems is strongly influenced by the properties of support.

Acknowledgements

We gratefully acknowledge the financial supports from the Ministry of Science and Technology of China (No. 2006AA060306, 2009AA064804).

References

[1] A. Papavasiliou, A. Tsetsekou, V. Matsouka, M. Konsolakis, I.V. Yentekakis, N. Boukos, Appl. Catal. B 90 (2009) 162–174.
[2] A. Kubacka, A. Martínez-Arias, M. Fernández-García, M.A. Newton, Catal. Today 145 (2009) 288–293.
[3] A. Winkler, P. Dimopoulos, R. Hauert, C. Bach, M. Aguirre, Appl. Catal. B 84 (2008) 162–169.
[4] M. Salaün, A. Kouakou, S. Da Costa, P. Da Costa, Appl. Catal. B 88 (2009) 386–397.
[5] V. Matsouka, M. Konsolakis, R.M. Lambert, I.V. Yentekakis, Appl. Catal. B 84 (2008) 715–722.
[6] L.F. Liotta, A. Longo, G. Pantaleo, G. Di Carlo, A. Martorana, S. Cimino, G. Russo, G. Deganello, Appl. Catal. B 90 (2009) 470–477.
[7] T. Kobayashi, T. Yamada, K. Kayano, Appl. Catal. B 30 (2001) 287–292.
[8] C. Larese, M. López Granados, F. Cabello Galisteo, R. Mariscal, J.L.G. Fierro, Appl. Catal. B 62 (2006) 132–143.
[9] M.V. Twigg, Appl. Catal. B 70 (2007) 2–15.
[10] I. Atribak, A. Bueno-López, A. García-García, J. Catal. 259 (2008) 123–132.
[11] D.S. Lafyatis, G.P. Ansell, S.C. Bennett, J.C. Frost, P.J. Millington, R.R. Rajaram, A.P. Walker, T.H. Ballinger, Appl. Catal. B 18 (1998) 123–135.
[12] J. Fan, X. Wu, X. Wu, Q. Liang, R. Ran, D. Weng, Appl. Catal. B 81 (2008) 38–48.
[13] Z. Hu, C.Z. Wan, Y.K. Lui, J. Dettling, J.J. Steger, Catal. Today 30 (1996) 83–89.
[14] M. Skoglundh, H. Johansson, L. Löwendahl, K. Jansson, L. Dahl, B. Hirschauer, Appl. Catal. B 7 (1996) 299–319.
[15] X. Weng, B. Perston, X.Z. Wang, I. Abrahams, T. Lin, S. Yang, J.R.G. Evans, D.J. Morgan, A.F. Carley, M. Bowker, J.C. Knowles, I. Rehman, J.A. Darr, Appl. Catal. B 90 (2009) 405–415.
[16] A. Iglesias-Juez, A.B. Hungría, A. Martínez-Arias, J.A. Anderson, M. Fernández-García, Catal. Today 143 (2009) 195–202.
[17] J. Luo, M. Meng, J. Yao, X. Li, Y. Zha, X. Wang, T. Zhang, Appl. Catal. B 87 (2009) 92–103.
[18] X. Courtois, V. Perrichon, Appl. Catal. B 57 (2005) 63–72.
[19] L. Jia, M. Shen, J. Wang, X. Chu, J. Wang, Z. Hu, J. Rare Earths 26 (2008) 523–527.
[20] A.B. Hungría, N.D. Browning, R.P. Erni, M. Fernández-García, J.C. Conesa, J.A. Pérez-Omil, A. Martínez-Arias, J. Catal. 235 (2005) 251–261.
[21] A.B. Hungría, M. Fernández-García, J.A. Anderson, A. Martínez-Arias, J. Catal. 235 (2005) 262–271.
[22] A. Martínez-Arias, M. Fernández-García, A.B. Hungría, A. Iglesias-Juez, J.A. Anderson, Catal. Today 126 (2007) 90–95.
[23] D. Terribile, A. Trovarelli, C. de Leitenburg, A. Primavera, G. Dolcetti, Catal. Today 47 (1999) 133–140.
[24] A. Elhamdaoui, G. Bergeret, J. Massadier, M. Primet, A. Renouprez, J. Catal. 148 (1994) 47–55.
[25] M. Fernández-García, A. Martínez-Arias, C. Belver, J.A. Anderson, J.C. Conesa, J. Soria, J. Catal. 190 (2000) 387–395.
[26] A.B. Hungría, A. Iglesias-Juez, A. Martínez-Arias, M. Fernández-García, J.A. Anderson, J.C. Conesa, J. Soria, J. Catal. 206 (2002) 281–294.
[27] S. Yamamoto, K. Matsushita, Nippon Kagaku Kaishi 8 (2000) 553–561.
[28] A.B. Hungría, J.J. Calvino, J.A. Anderson, A. Martínez-Arias, Appl. Catal. B 62 (2006) 359–368.
[29] P.S. Lambrou, P.G. Savva, J.L.G. Fierro, A.M. Efstathiou, Appl. Catal. B 76 (2007) 375–385.
[30] E. Aneggi, C. de Leitenburg, G. Dolcetti, A. Trovarelli, Catal. Today 114 (2006) 40–47.
[31] C. Li, X. Gu, Y. Wang, Y. Wang, Y. Wang, X. Liu, G. Lu, J. Rare Earths 27 (2) (2009) 211–215.
[32] A.I. Kozlov, D.H. Kim, A. Yezerets, P. Andersen, H.H. Kung, M.C. Kung, J. Catal. 209 (2002) 417–426.
[33] C. Larese, M. López Grandos, R. Mariscal, J.L.G. Fierro, P.S. Lambrou, A.M. Efstathiou, Appl. Catal. B 59 (2005) 13–25.
[34] H. Birgersson, M. Boutonnet, F. Klingstedt, D.Yu. Murzin, P. Stefanov, A. Naydenov, Appl. Catal. B 65 (2006) 93–100.
[35] M. López Granados, A. Gurbani, R. Mariscal, J.L.G. Fierro, J. Catal. 256 (2008) 172–182.
[36] J. Fan, D. Weng, X. Wu, X. Wu, R. Ran, J. Catal. 258 (2008) 177–186.
[37] J. Wang, M. Shen, Y. An, J. Wang, Catal. Commun. 10 (2008) 103–107.
[38] M. Zhao, M. Shen, J. Wang, J. Catal. 248 (2007) 258–267.
[39] R.A. Daley, S.Y. Christou, A.M. Efstathiou, J.A. Anderson, Appl. Catal. B 60 (2005) 117–127.
[40] P.S. Lambrou, A.M. Efstathiou, J. Catal. 240 (2006) 182–193.
[41] G. Chen, W.T. Chou, C.T. Yeh, Appl. Catal. 8 (1983) 389–397.
[42] H. Vidal, J. Kašpar, M. Pijolat, G. Colon, S. Bernal, A. Cordón, V. Perrichon, F. Fally, Appl. Catal. B 30 (2001) 75–85.
[43] P. Fornasiero, R. Di Monte, G.R. Rao, J. Kašpar, S. Meriani, A. Trovarelli, M. Graziani, J. Catal. 151 (1995) 168–177.
[44] I. Heo, J.W. Choung, P.S. Kim, I.-S. Nam, Y. Song, C.B. In, G. Yeo, Appl. Catal. B 92 (2009) 114–125.
[45] P. Fornasiero, E. Fonda, R. Di Monte, G. Vlaic, J. Kašpar, M. Graziani, J. Catal. 187 (1999) 177–185.
[46] P. Fornasiero, J. Kašpar, M. Graziani, Appl. Catal. B 22 (1999) L11–L14.
[47] X. Wu, J. Fan, R. Rui, D. Weng, Chem. Eng. J. 109 (2005) 133–139.